Artificial Organs
26(7):590–599, Blackwell Publishing, Inc.

Computational Flow Modeling in Hollow-Fiber Dialyzers

Sunny Eloot, Dirk De Wachter, IlseVan Tricht, and Pascal Verdonck

Hydraulics Laboratory, Institute of Biomedical Technology, Ghent University, Gent, Belgium

Abstract: A three-dimensional finite volume model of the blood-dialysate interface over the complete length of the dialyzer was developed. Different equations govern dialyzer flow and pressure distribution (Navier-Stokes) and radial transport (Darcy). Blood was modeled as a non-Newtonian fluid with a viscosity varying in radial and axial direction determined by the local hematocrit, the diameter of the capillaries, and the local shear rate. The dialysate flow was assumed to be an incompressible, isothermal laminar Newtonian flow with a constant viscosity. The permeability characteristics of the membrane were calculated from laboratory tests for forward and backfiltration. The oncotic pressure induced by the plasma proteins was implemented as well as the reduction of the overall permeability caused by the adhesion of proteins to the membrane. From the calculated pressure distribution, the impact of flow, hematocrit, and capillary dimensions on the presence and localization of backfiltration can be investigated. **Key Words:** Dialyzer—Computational fluid dynamics—Blood viscosity—Ultrafiltration—Backfiltration.

This work contains 2 major sections. First, an extended literature review of numerical models related to flow and transport in hemodialyzers is given. Second, our three-dimensional numerical model is described in detail.

BACKGROUND

The pressure profile in the blood as well as in the dialysate compartment are determinants of backfiltration in hemodialyzers and gained considerable attention in recent years. In addition, the flow distribution in both compartments has a large impact on the mass transfer efficiency.

Whereas one can investigate and compute (macroscopically) blood and dialysate flow in a dialyzer assuming flow in a permeable medium, it should be noted that some important aspects like ultrafiltration, convection-diffusion, concentration polarization, particle accumulation or protein adsorption at the membrane surface, and the multiphasic blood flow should be investigated with a microscopic model. Computational fluid dynamics (CFD) is a useful tool for flow visualization at both the macroscopic and microscopic levels. However, the numerical results should be validated at least with analytical solutions and/or experimental measurements.

Received March 2002.
Address correspondence and reprint requests to Sunny Eloot, M.Sc., B.M.E., Hydraulics Laboratory, Institute of Biomedical Technology, Ghent University, St.-Pietersnieuwstraat 41, 9000 Gent, Belgium. E-mail: Sunny.Eloot@rug.ac.be

Blood and dialysate flow

Nordon and Shindhelm (1) investigated with a finite volume software package (Fluent 4) the parameters influencing the flow distribution in an axisymmetrical two-dimensional (2D) model of the blood compartment of hollow-fiber systems used for affinity cell separation. In the inlet and outlet header region, the Navier-Stokes (momentum) equations were solved for steady incompressible laminar flow, while the hollow fibers were modeled as a porous medium with a radial permeability factor of 3 less than the axial permeability. In the upstream header, boundary layer separation occurred at the point of channel divergence causing the formation of a separation bubble, a finding that was confirmed in an analogous numerical study for hemodialyzers (2). Moreover, both studies (1,2) found that the uniformity of the porous medium flow mainly is influenced by the radial-to-axial hydraulic permeability ratio.

Osuga et al. (3) determined dialysate pressure isobars in a low flux hollow-fiber dialyzer (Toray B2-2.0) by combining the results of magnetic resonance imaging and a numerical simulation of the injected contrast solution in the dialysate flow. The latter was regarded as a porous medium flow depending on the

radial-to-axial hydraulic permeability ratio which was determined by comparing the results of both measuring techniques. The a priori assumption that the ultrafiltration flux into the dialysate can be ignored is supported by the finding that the isobars have no steep radial gradient such that a homogeneous flow pattern can be assumed. However, Takesawa et al. (4) found, using x-ray computed tomography (CT), a radially distributed dialysate flow due to the breaking and twisting of fiber bundles made of cellulosic membrane. On the other hand, using a helical CT scan, Ronco et al. evaluated the use of spacing filaments (5) and hollow fibers with a moiré structured wave design (6) (Nissho FB130). They found those techniques were effective in preventing the fiber twisting, thereby resulting in an idealized dialysate flow pattern without dialysate channeling. Spacing filaments used in flat dialyzers, simulated with a three-dimensional (3D) steady state CFD model by Karode and Kumar (7), or in coil dialyzers, play an important role in the promotion of fluid mixing and thus reducing concentration polarization by increasing the shear rate at the membrane surface (8). In summary, the fact whether the dialysate flow distribution is homogeneous or not mainly is influenced by the dialyzer type with respect to fiber twisting.

Using magnetic resonance Fourier velocity imaging to determine the blood and dialysate flow distributions simultaneously, Zhang et al. (9) found a uniform blood and nonuniform dialysate flow distribution.

Ultrafiltration: Haegen-Poiseuille

Ultrafiltration, generated by osmotic and hydrostatic pressure drops over a porous membrane, originally was described numerically by Kedem and Katchalsky (10) using thermodynamics of irreversible processes. The membrane properties were described in terms of filtration, reflection, and permeability. Rather than using thermodynamics, Kargol (11) redefined those coefficients assuming a membrane with randomly distributed pore sizes. Using a theoretical model validated with experiments, Wüpper et al. (12) described the profile of ultrafiltration and concentration along the axis of high flux hollow-fiber dialyzers. It was found that the hydrostatic pressure profile could be approximated as linear even in the presence of a nonlinear concentration profile for impermeable solutes. As a result, changes in fiber radius and membrane permeability can be studied using the Darcy and Haegen-Poiseuille laws.

Karode (13) derived analytical expressions for the pressure drop in a permeable tube as a function of wall permeability, channel dimensions, axial position, and fluid properties by differentiating the Haegen-Poiseuille formula and applying it locally to infinitesimal sections. Moreover, to benchmark the expression for constant wall permeability, a CFD model (Phoenics) was developed and verified by comparing the results for constant wall velocity with Berman's (14) solution.

Mass transport: convection-diffusion

In hemodiafiltration, toxic agents are removed by a combination of diffusion and convection resulting in a better clearance of high molecular weight (HMW) solutes while maintaining the performance for low molecular weight (LMW) solutes. In several studies (12,15–21) transport phenomena in hemodiafilters have been described based on the assumption of a constant ultrafiltration flow (15–17,19) and neglecting the accumulation of partially rejected solutes at the membrane wall (15,17). Jaffrin (20) and Zydney (22) found that the convective contribution of HMW solutes partially rejected by the membrane is larger than expected and, in the case of dominant ultrafiltration, is independent of the sieving coefficient. Others (16–18,20) investigated the solute transport accounting for the module geometry, the membrane properties, and the operating conditions but without considering the effective ultrafiltration profile along the dialyzer length nor the change of the mass transfer coefficient. On the other hand, Legallais et al. (23) incorporated those aspects and the concentration polarization aspect in a one-dimensional (1D) transport model for hemodiafilters using Newtonian fluids and assuming the desired ultrafiltration rate. Pressure in both compartments was assumed to drop following the Haegen-Poiseuille equation applied to an equivalent cylindrical tube (24) and using local fluid viscosities.

Assuming diffusion to be more dominant than convection, Jaffrin et al. (18) found that the assumption of a linear concentration profile in boundary layers is only valid for LMW solutes while it should be assumed rather exponential in the case of HMW solutes. Grimsrud and Babb (25) and Colton et al. (26) investigated the concentration profile for diffusion in blood flowing through 2 infinite flat plates respectively at the entrance region, assuming zero ultrafiltration. Berman (14) solved the Navier-Stokes equations asymptotically for small constant ultrafiltration values. Because the assumption of a zero or constant ultrafiltration velocity was not realistic, Ross (27) analyzed the mass transport in a laminar Newtonian fluid flow through a permeable tubular membrane. He used an ultrafiltration velocity

depending on hydrostatic and osmotic pressure differences while the solute transport was determined by the reflection coefficient of the membrane.

For the investigation of mass transport in dialyzers, most authors neglect or simplify the ultrafiltration aspect, while others (23,27) take into account a linear pressure distribution over the length of the dialyzer, determining the ultrafiltration profile.

Concentration-polarization

In the presence of ultrafiltration, particles within the main stream are subjected to a drag force and accumulate near the membrane surface while the accumulated particles tend to migrate to the feeding stream driven by the concentration gradient. The boundary layer concentration modifies the solute and/or solvent properties like viscosity, density, and solute molecular diffusivity (28). Due to particle accumulation, ultrafiltration flow decreases with time and a steady state value, described as a function of the concentration ratio near the membrane and in the main stream and of the mass transfer coefficient, was derived by Michaels (29) using the 1D convection-diffusion equation. Backfiltration, caused by the oncotic effect, induces a shear stress that was incorporated by Zydney and Colton (30) by using the shear-induced hydrodynamic diffusion coefficient analyzed experimentally by Eckstein et al. (31). Moreover, the shear stress, maximal at the membrane on the fluid-like concentrated layer, causes this layer to get fluidized. This shear-induced hydrodynamic diffusion process was implemented by Romero and Davis (32) taking into account the 2D characteristics of ultrafiltration by integrating the axial momentum equation into the 1D convection-diffusion equation.

Lee and Clark (33) used the 2D convection-diffusion equation to describe, using an iterative algorithm, the ultrafiltration flow decline caused by concentration polarization. They found that the concentration as well as the thickness of the boundary layer increases with axial distance but decreases for higher diffusion coefficients and axial velocities.

For computational modeling of such a thin boundary layer in which the solute concentration changes intensively, a very dense grid should be used. To enable the use of a large grid, Miranda and Campos (28) applied a simple natural logarithmic variable transformation, a procedure described earlier by Zydney (34), in the solute transport equation attenuating the concentration derivatives inside the boundary layer. Other studies (35,36) refer to the use of CFD to model concentration polarization in the fluid phase adjacent to the membrane without taking into account the selective permeation through the membrane fluid phase.

Particle accumulation

Because the characteristics of the particle layer on the membrane are related directly to the hydraulic permeability, numerous algorithms (e.g., based on a simple Monte Carlo simulation [37] or a discrete stochastic model [38]) exist for simulating the particle packing. Kawakatsu et al. (39) performed a 3D analysis of boundary layer formation and porosity assuming monodispersed particles moving according to Brownian motion. Emphasizing the nonequal sized character of accumulating particles, Yoon et al. (40) developed a 3D simulation for the microfiltration of colloidal particles considering the particle backtransport velocity that was found to be dominantly controlled by particle-surface interactions. The particle transport toward the membrane surface was determined considering the ensemble of forces (lift, drag, van der Waals attraction, and charge repulsion) and torques acting on the moving particle. Moreover, the flux is calculated using the concept of a resistance in series model considering pore blocking as well as layer resistance. For nonflocculating particle conditions, the latter is the major flux controlling parameter.

Multiphase flow

The unidirectional shear flow of highly concentrated fluid-particle suspensions, showing particle migration from regions of high shear to regions of low shear, has been investigated using a 2D (41) and axisymmetric (42) numerical model. The suspension, treated as a Newtonian fluid, is modeled using the momentum and continuity equation, whereas the particle motion is governed by a modified transport equation accounting for the effects of shear-induced particle migrations. Although the parameters of rigid neutrally buoyant particles (42) are far from matching those of the deformable red blood cells, the numerical results, in good agreement with analytical predictions of Phillips et al. (43), may contribute to a better understanding of the possible local variations of the hematocrit.

NUMERICAL MODEL

A 3D finite volume microscopic model of the blood-dialysate interface over the complete length of a dialyzer has been developed (Fluent 5.4, Sheffield, U.K.). Assuming the fibers spaced in a hexagonal lattice and based on symmetry, a twelfth part of 1 single fiber can be isolated (Fig. 1). The parameter settings of the 3D module (Fig. 2) were assessed for

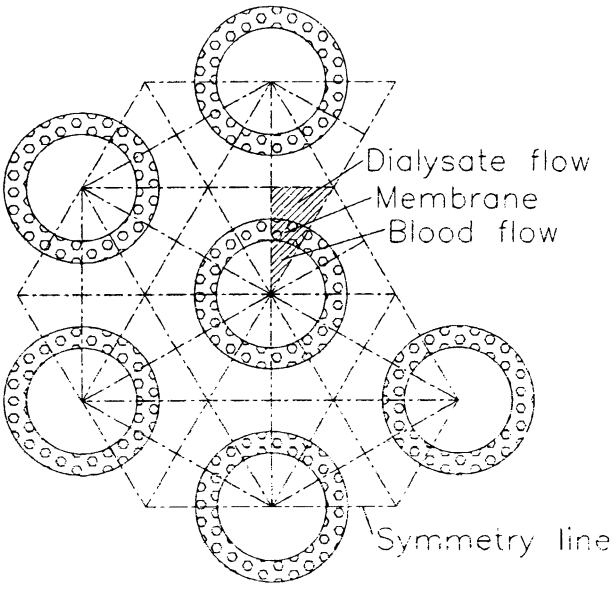

FIG. 1. The drawing is of the hexagonal lattice of the hollow-fiber dialyzer (cross section).

a high flux polysulphone Fresenius F60, characterized by a fiber diameter of 200 μm, membrane thickness of 40 μm (1 μm inner layer and 39 μm bulk layer), and dialysate compartment dimensions (maximum radius 230 μm) calculated from fiber density. The membrane module has an active length of 230 mm while inlet and outlet tubes (each 12.5 mm long) are forseen in both fluid compartments simulating the header and potting regions. For the implementation in the numerical model, properties of the 3 compartments, blood, dialysate, and the semipermeable membrane in between, are derived from in vitro and in vivo tests.

Membrane permeability

The permeability characteristics of the membrane are obtained from laboratory tests in which a dialysate flow was forced through the membrane. The ultrafiltration coefficient (m^3/s.Pa) is calculated from flow (m^3/s) and transmembrane pressure (Pa) measurements. Furthermore, the hydraulic membrane permeability (m^2/s.Pa) is derived from the ultrafiltration coefficient, membrane surface, and thickness. The tests are done for forward and backfiltration using sterile dialyzers (overall permeability 7,950 nm^2/s.Pa) as well as samples in which a protein layer is induced on the membrane (overall permeability 2,400 nm^2/s.Pa) simulating a clinical session (44). The permeabilities of a sterile inner layer and bulk layer are implemented as a series of 2 resistances whereas the influence of a protein layer on the overall membrane permeability is incorporated as a higher resistive inner layer.

Dialysate fluid properties

From bicarbonate dialysate samples taken in vivo from the supply and the drain of the dialyzer, dynamic viscosity and density were determined using a capillary Ubbelohde viscosimeter and a density-hydrometer-aerometer, respectively. Because it was found that both properties are not influenced by the dialysis session, the dialysate flow is assumed as an incompressible, isothermal laminar Newtonian flow with a constant viscosity (0.687 mPa.s) and density (1,008 kg/m^3).

Non-Newtonian blood behavior

An extended literature review was needed to perform an accurate modeling of the non-Newtonian blood flow. While plasma or another Newtonian fluid is used in the blood compartment for the majority of the models described in the literature (23,27), the presented model accounts for the influence on viscosity of the local hematocrit, the small diameter of the capillaries, and the local shear rate.

The shear thinning behavior as well as the depen-

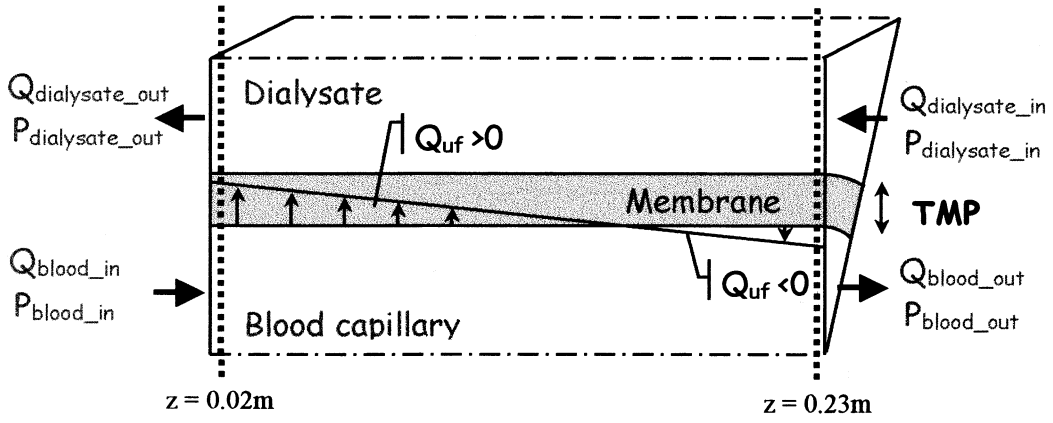

FIG. 2. Shown is a 3D visualization of an isolated unit (blood, membrane, and dialysate compartment).

dence of the blood viscosity μ on the local hematocrit H, is described by Quemada (45):

$$\mu = \frac{\mu_{plasma}}{\left(1 - \frac{1}{2} k \times H\right)^2} \quad (1)$$

Parameter k is a function of the intrinsic viscosities $k_0(H)$, characterizing the red blood cell aggregation at zero shear stress, $k_\infty(H)$, describing the orientation and deformation of red blood cells at important shear stress, and the shear rate γ. For a fixed hematocrit, viscosity decreases with increasing shear rate, whereas for a fixed shear rate, viscosity increases with hematocrit.

Blood flowing through small capillaries exhibits a redistribution of the red blood cells in such a way that a plasma skimming layer can be observed near the wall while red blood cells are concentrated in the center. Fahraeus and Lindqvist (46) described the effect of this nonuniform cell distribution on the flow by defining an apparent blood viscosity for use in the Haegen-Poiseuille equation. The radial variation of the hematocrit was deduced by Lerche and Roelke (47) using a parameter n that describes the degree of plasma skimming. Nonuniformity of cell distribution increases with decreasing n. This parameter is determined iteratively as a function of the hematocrit using an axisymmetrical numerical model such that the obtained viscosity for flow in a small tube matches literature results of the apparent viscosity (Fig. 3).

Because plasma density (1,030 kg/m^3) differs from the density of platelets and blood cells (1,090 kg/m^3), the density of blood ρ_{blood} varies with the local hematocrit H:

$$\rho_{blood} = 1030 \times (1 - H) + 1090 \times H \quad (kg/m^3) \quad (2)$$

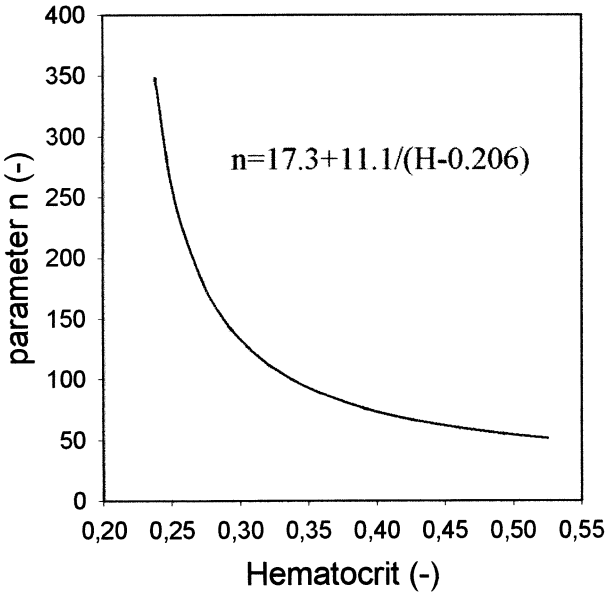

FIG. 3. The graph shows Lerche parameter n as a function of hematocrit.

Governing equations

In the blood and dialysate compartment, conservation of mass and momentum are described by the 3D steady incompressible Navier-Stokes and continuity equations, using the local and constant viscosity and density for blood and dialysate, respectively. The transmembrane water transport, function of the membrane permeability, and the local oncotic pressure are described by the Darcy equation for porous media.

Boundary conditions

In the blood and dialysate compartment, a constant inlet velocity is given while outlet conditions can be specified either as outlet pressures or as a flow percentual distribution in both compartments to apply the desired ultrafiltration flow. Oncotic pressure, which is exerted by the plasma proteins and opposes the hydrostatic transmembrane pressure, is implemented as a discontinuous pressure drop at the skin-bulk interface. Moreover, as hemoconcentration takes place in axial direction, the oncotic pressure is varying with hematocrit. Because the smallest blood-membrane-dialysate entity was isolated, all other boundaries are symmetry planes.

RESULTS

Assuming a constant blood and dialysate inlet flow of 250 and 500 ml/min, respectively, outlet pressures of 10 kPa and 5 Pa, respectively, and initial oncotic pressure of 3.33 kPa, the pressure distribution renders an overall ultrafiltration flow of 45 ml/min while no backfiltration occurs (Figs. 4 and 6).

As blood, with an initial viscosity of 3 mPa.s, flows through the dialyzer, the water removal causes hemoconcentration. As a consequence, the bulk hematocrit shows an axial variation from its initial value 0.30 at blood entrance up to 0.42 at the outlet, resulting in a mean viscosity increase from 3 mPa.s to 4.5 mPa.s. The plug flow of blood cells at the axis (maximum viscosity 7.5–11.8 mPa.s) and the plasma layer near the membrane wall (viscosity 1.3 mPa.s) demonstrates the radial variation of the blood viscosity (Fig. 5).

The oncotic pressure, varying with the local hematocrit, increases from its initial value 3.33 kPa up to 4.20 kPa. The ultrafiltration flow is decreased by

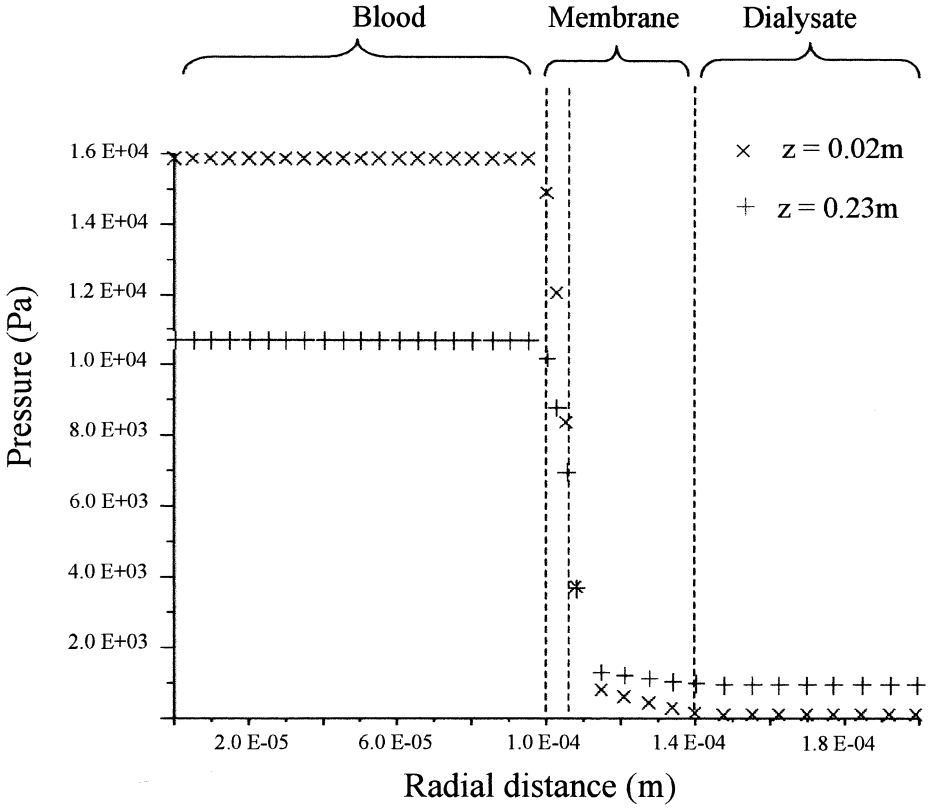

FIG. 4. Shown is the radial pressure distribution at the blood inlet (×) and outlet (+) section.

28% because of the oncotic pressure opposing the hydraulic driving pressure.

The shear stress, zero at blood and dialysate axes, is maximal at the blood-membrane interface, decreasing from 0.97 Pa at blood inlet to 0.78 Pa at the outlet, while it is slightly increasing at the dialysate-membrane interface from 0.23 up to 0.26 Pa at the dialysate outlet.

Due to ultrafiltration, one may expect a deviation from the linear flow-pressure drop profile described by Haegen-Poiseuille as well as from the parabolic velocity profile. Nevertheless, for an ultrafiltration flow of 45 ml/min in a dialyzer module of 230 mm, the pressure distribution in the blood compartment deviates only slightly from linearity (maximum 0.28% to 0.33% at the blood inlet and outlet, respectively) (Fig. 6) while the same is true for the parabolic velocity profile (R^2 = 0.997–0.993 at the blood inlet and outlet respectively) (Fig. 7).

DISCUSSION

The presented 3D microscopic model allows the investigation of the impact of flow, blood viscosity, and hematocrit on the presence and localization of backfiltration for given capillary dimensions. Varying the dimensions of the dialysate compartment subsequently, the impact of anisotropic fiber density and/or fiber twisting, as reported in macroscopic models (4,5,7), can be investigated. Moreover, the influence of a nonuniform blood and/or dialysate flow (1,2,4,5,7,9), resulting in locally different ultrafiltration flows, can be visualized at discrete radial positions.

In the 1D model of Legallais et al. (23), hydraulic and diffusive permeabilities of the membrane are obtained from experimental results found in the literature (18,48). In contrast with experiments where the hydraulic permeability (18,48,49) and the influence of proteins (48) is investigated in an ex vivo set-up using the clinical flow directions, a new in vitro set-up was built for this study in order to quantify the water permeability of the membrane as its real physical characteristic with greater accuracy. Nevertheless, the plasma ultrafiltration coefficient found by Bosch et al. (48) in their ex vivo set-up shows a permeability reduction of 68% compared with their sodium chloride measurements, quite similar to what we measure after inducing an in vitro protein layer on the dialyzer membrane (reduction of 70%).

Legallais et al. (23) assumed the Newtonian fluid plasma to flow in the blood compartment with a viscosity depending on the actual protein concentration

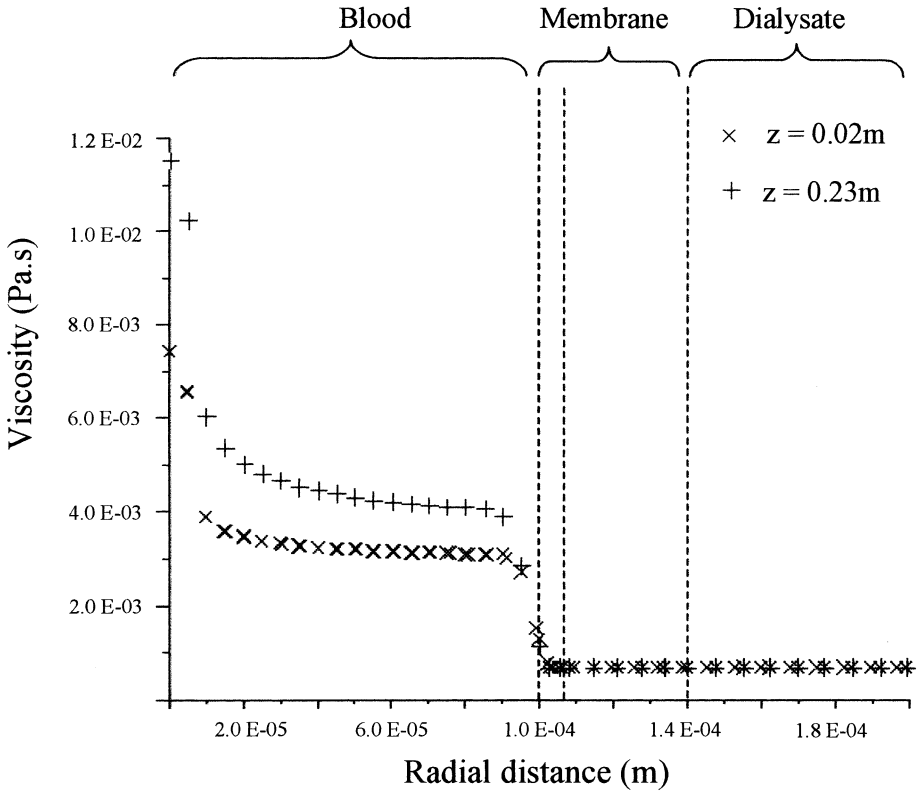

FIG. 5. Shown is the radial viscosity distribution at the blood inlet (×) and outlet (+) section.

(50). In the presented model, the shear-thinning behavior of blood as well as the hematocrit dependency of its viscosity is incorporated using the Quemada model (45). The influence of the nonuniform cell distribution is taken into account by using the Fahraeus-Lindqvist model, which was originally derived for impermeable tubes.

Oncotic pressure, induced by the plasma proteins in the blood compartment, is not considered in models using saline solutions. For plasma (23), the oncotic pressure dependence on protein concentration is expressed by Landis and Pappenheimer (51). In our study, using blood, the local oncotic pressure is calculated accounting for the local hematocrit. As

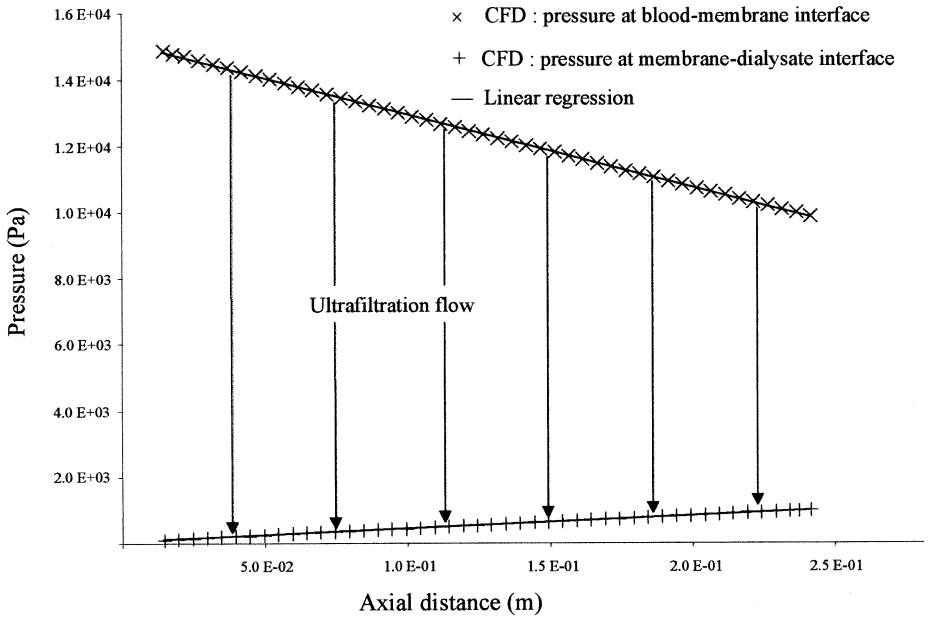

FIG. 6. Shown is the axial pressure distribution in the blood (×) and dialysate (+) compartment.

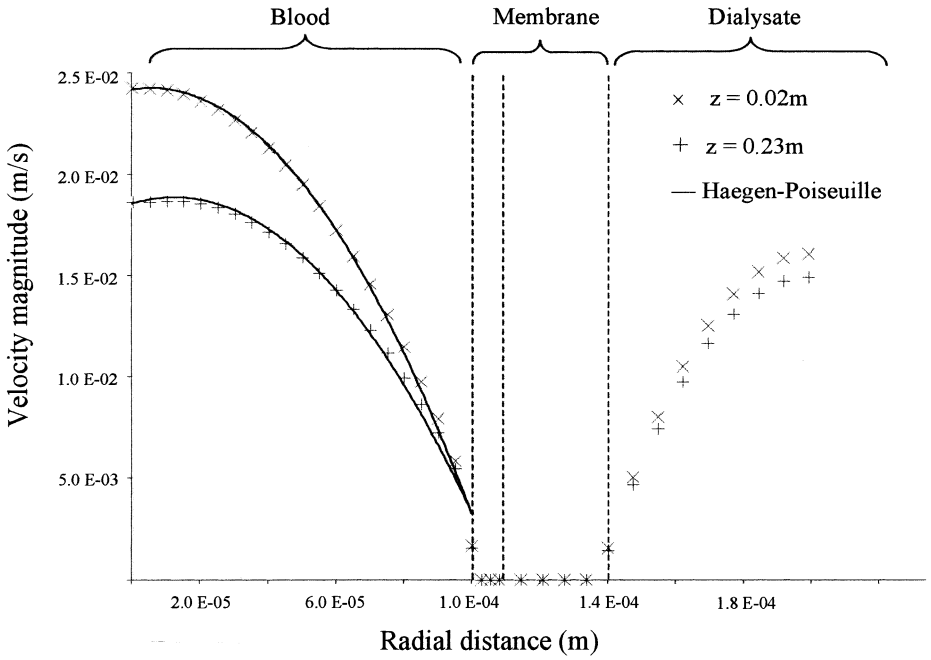

FIG. 7. Shown is the spatial velocity profile in the blood and dialysate compartment at the blood inlet (×) and outlet (+) section.

water is removed from the blood compartment over the length of the dialyzer and hemoconcentration occurs, the local hematocrit increases with the red blood cell concentration and the oncotic pressure increases with protein (albumin) concentration.

Although the Haegen-Poiseuille equation is derived for flow in impermeable tubes, most 1D and 2D numerical models (23) assume a linear pressure drop over the length of the dialyzer. Our 3D model gives the opportunity to investigate whether this assumption is valid. It is found (Figs. 6 and 7) that deviation from linearity is negligible (0.3%) for flow in dialyzers with a limited active length (230 mm), hereby confirming the theoretical results by Wüpper et al (12). However, using the analytical expression of Karode (13), a deviation from linearity of 6% is found at the blood inlet and outlet for a common active dialyzer length (0.23 m).

After validation of the model by an ex vivo study mimicking the clinical set-up, a profound parameter study can be performed to investigate the impact of ultrafiltration flow and capillary dimensions on blood viscosity.

Although the presented model is the result of combining several flow, transport, and fluid property aspects, some limitations of the model can be remarked upon. Concentration polarization, which should be considered for flow in permeable tubes, is not considered. Moreover, the accumulation of particles at the membrane is idealized by assuming the presence of a homogeneous monolayer of proteins (100 nm) at the inner layer of the membrane. As a result, the axial variation of boundary layer thickness (33) and the shearing effect arising from backfiltration (30,31) as well as the shear stress acting on the boundary layer itself (32) are not considered. Therefore, with respect to the flow of highly concentrated fluids like blood, the consideration of concentration polarization and multiphasic flow simulating inertial effects and slip between the particles and the carrier liquid (44) could be a point of further improvement.

CONCLUSIONS

Our numerical model incorporates the blood, dialysate, and membrane flow in hollow-fiber dialyzers allowing an accurate investigation of the fluid properties and the presence and localization of backfiltration can be performed. The hydraulic permeability of the dialyzer is based on a different and more accurate method than in previous ex vivo studies, and blood is modeled as a non-Newtonian fluid with properties varying in the radial as well as axial direction. The simulation shows that deviation from a linear pressure drop–flow relationship is negligible for flow in dialyzers with a limited active length.

Acknowledgments: This research was financially supported by Fresenius Medical Care (Bad Homburg, Germany). The authors also thank the medical staff of the renal unit of the hospital "A.Z. Zusters van Barmhartigheid" (Ronse, Belgium) for their assistance during the in vivo measurements, the Blood Transfusion Center (Red Cross Belgium) for supplying plasma pockets used in the laboratory tests and, last but not least, our colleague Patrick Segers for his review.

REFERENCES

1. Nordon RE, Schindhelm K. Design of hollow fiber modules for uniform shear elution affinity cell separation. *Artif Organs* 1997;21:107–15.
2. Eloot S, Dierickx P, Bouwens L, Cuvelier B, Dierckx R, Verdonck P. Blood flow visualisation in a hollow fiber dialyser using CFD and SPECT. Scientific Meeting SBN-BVN 2001;14.
3. Osuga T, Obata T, Ikehira H, Tanada S, Sasaki Y, Naito H. Dialysate pressure isobars in a hollow-fiber dialyzer determined from magnetic resonance imaging and numerical simulation of dialysate flow. *Artif Organs* 1998;22:907–9.
4. Takesawa S, Terasawa M, Sakagami M, Kobayashi T, Hidai H, Sakai K. Nondestructive evaluation by x-ray computed tomography of dialysate flow patterns in capillary dialysers. *Trans Am Soc Artif Organs* 1988;34:794–9.
5. Ronco C, Scabardi M, Goldoni M, Brendolan A, Crepaldi C, La Greca G. Impact of spacing filaments external to hollow fibers on dialysate flow distribution and dialyzer performance. *Int J Artif Organs* 1997;20:261–6.
6. Ronco C, Brendolan A, Crepaldi C, Rodighiero M, Everard P, Ballestri M, Capelli G, Spittle M, La Greca G. Dialysate flow distribution in hollow fiber hemodialyzers with different dialysate pathway configurations. *Int J Artif Organs* 2000;23: 601–9.
7. Karode SK, Kumar Q. Flow visualisation through spacer filled channels by computational fluid dynamics I. Pressure drop and shear rate calculations for flat sheet geometry. *J Membr Sci* 2001;193:69–84.
8. Da Costa AR, Fane AG, Fell CJD, Franken ACM. Optimal channel spacer design for ultrafiltration. *J Membr Sci* 1991; 62:275–91.
9. Zhang J, Parker DL, Leypoldt JK. Flow distribution in hollow fiber hemodialysers using magnetic resonance Fourier velocity imaging. *ASAIO J* 1995;41:M678–82.
10. Kedem O, Katchalsky A. Thermodynamic analysis of the permeability of biological membranes to non-electrolytes. *Biochim Biophys Acta* 1958;27:229–46.
11. Kargol A. A mechanistic model of transport processes in porous membranes generated by osmotic and hydrostatic pressure. *J Membr Sci* 2001;191:61–9.
12. Wüpper A, Dellanna F, Baldamus CA, Woermann D. Local transport processes in high-flux hollow fiber dialyzers. *J Membr Sci* 1997;131:181–93.
13. Karode SK. Laminar flow in channels with porous walls, revisited. *J Membr Sci* 2001;191:237–41.
14. Berman A. Laminar flow in channels with porous walls. *J Appl Phys* 1953;24:1232–5.
15. Abbas M, Tyagi VP. On the mass transfer in a circular conduit dialyzer when ultrfiltration is coupled with dialysis. *Int J Heat Mass Transfer* 1988;31:591–602.
16. Yaffrin MY, Gupta BB, Malbrancq JM. A one-dimensional model of simultaneous hemodialysis and ultrafiltration with highly permeable membranes. *J Biomech Eng* 1981;103:261–6.
17. Sigdell JE. Calculation of combined diffusive and convective mass transfer. *Int J Artif Organs* 1982;5:361–72.
18. Jaffrin MY, Ding LH, Laurent JM. Simultaneous convective and diffusive mass transfer in a hemodialyser. *J Biomech Eng* 1990;112:212–9.
19. Werynski A, Wanieski J. Theoretical description of mass transport in medical devices. *Artif Organs* 1995;19:420–7.
20. Jaffrin MY. Convective mass transfer in hemodialysis. *Artif Organs* 1995;19:1162–71.
21. Wüpper A, Woermann D, Dellanna F, Baldamus CA. Retrofiltration rates in high-flux hollow fibers hemodialysers: Analysis of clinical data. *J Membr Sci* 1996;121:109–16.
22. Zydney AL. Bulk mass transport limitations during high flux hemodialysis. *Artif Organs* 1993;17:919–24.
23. Legallais C, Catapano G, von Harten B, Baurmeister U. A theoretical model to predict the in vitro performance of hemodiafilters. *J Membr Sci* 2000;168:3–15.
24. Hosoya N, Sakai K. Backdiffusion rather than backfiltration enhances endotoxin transport through highly permeable dialysis membranes. *Trans ASAIO* 1990;36:M311–3.
25. Grimsrud L, Babb AL. Velocity and concentration profiles for laminar flow of a newtonian fluid in a dialyser. *Chem Eng Prog* 1966;62:20–31.
26. Colton C, Smith K, Stroeve P, Merril E. Laminar flow mass transfer in a flat duct with permeable walls. *Am Inst Chem Eng* 1971;17:773–80.
27. Ross SM. A mathematical model of mass transport in a long permeable tube with radial convection. *J Fluid Mech* 1974;63: 157–75.
28. Miranda JM, Campos JBLM. An improved numerical scheme to study mass transfer over a seperation membrane. *J Membr Sci* 2001;188:49–59.
29. Michaels AS. New seperation technique for the CPI. *Chem Eng Prog* 1968;64:31–40.
30. Zydney AL, Colton CK. A concentration polarization model for the filtrate flux in cross-flow microfiltration of particulate suspensions. *Chem Eng Commun* 1986;47:1–21.
31. Eckstein EC, Bailey DG, Shapiro AH. Self-diffusion of particles in shear flow of a suspension. *J Fluid Mech* 1974;79: 191–208.
32. Romero CA, Davis RH. Global-model of cross-flow microfiltration based on hydrodynamic particle diffusion. *J Membr Sci* 1988;39:157–85.
33. Lee Y, Clark MM. A numerical model of steady-state permeate flux during cross-flow ultrafiltration. *Desalination* 1997; 109:241–51.
34. Zidney AL. Stagnant film model for concentration polarization in membrane systems. *J Membr Sci* 1997;130:275–81.
35. Bhattacharyya D, Back SL, Kermode RI. Prediction of concentration polarisation and flux behaviour in reverse osmosis by numerical analysis. *J Membr Sci* 1990;48:231–62.
36. Rosen C, Tragardh C. Computer simulation of mass transfer in the concentration boundary layer over ultrafiltration membranes. *J Membr Sci* 1993;85:139–56.
37. Vold MJ. Computer simulation of floc formation in a colloidal suspension. *J Colloid Sci* 1963;18:684–95.
38. Tassopoulos MJ, O'Brien JA, Rosner DE. Simulation of microstructure/mechanism relationships in particle deposition. *AIChE J* 1989;35:967–80.
39. Kawakatsu T, Nakajima M, Nakao S, Kimura S. Three-dimensional simulation of random packing and pore blocking phenomena during microfiltration. *Desalination* 1995;101: 203–9.
40. Yoon SH, Lee CH, Kim KJ, Fane AG. Three-dimensional simulation of the deposition of multi-dispersed charged particles and prediction of resulting flux during cross-flow microfiltration. *J Membr Sci* 1999;161:7–20.
41. Zhang K, Acrivos A. Viscous resuspension in fully developed laminar pipe flows. *Int J Multiphase Flow* 1994;20:579–91.
42. Hofer M, Perktold K. Computer simulation of concentrated fluid-particle suspension flows in axisymmetric geometries. *Biorheology* 1997;34:261–79.
43. Phillips RJ, Armstrong RC, Brown RA. A constitutive equation for concentrated suspensions that accounts for shear-induced particle migration. *Phys Fluids* 1992;4:30–40.
44. Eloot S, De Wachter D, Vienken J, Pohlmeier R, Verdonck P. In vitro evaluation of the hydraulic permeability of polysulfone dialysers. *Int J Artif Organs* (in press).
45. Quemada D. General features of blood circulation in narrow vessels. In: Rodkiewicz CM, ed. *Arteries and Arterial Blood Flows.* New York: Springer-Verlag, 1983.
46. Fahraeus R, Lindqvist T. The viscosity of blood in narrow capillary tubes. *Am J Physiol* 1931;96:562–68.
47. Lerche D, Roelke R. Theoretical model of blood flow through hollow fibers considering hematocrit-dependent,

non-Newtonian blood properties. *Int J Artif Organs* 1990;13: 742–6.
48. Bosch T, Schmidt B, Samtleben W, Gurland HJ. Effect of protein adsorption on diffusive and convective transport through polysulfone membranes. *Contrib Nephrol* 1985;46: 14–22.
49. Ronco C, Fabris A, Feriani M, Brendolan A, Chiaramonte S, La Greca G. Hydraulic properties and flow-dynamic characteristics of the new low flux polysulfone F6 membrane. *Contrib Nephrol* 1989;74:34–42.
50. Pallone TL, Terson J. A mathematical model of continuous arteriovenous hemofiltration predicts performance. *Trans ASAIO* 1987;33:304–8.
51. Landis EM, Pappenheimer JR, eds. *Handbook of Physiology, Section 2: Circulation*. Washington, DC: American Physiological Society, 1963:961.